THE ASTROPHYSICAL JOURNAL, 479:642–658, 1997 April 20

HUBBLE SPACE TELESCOPE IMAGES OF A SAMPLE OF 20 NEARBY LUMINOUS QUASARS[1]

JOHN N. BAHCALL, SOFIA KIRHAKOS, AND DAVID H. SAXE
Institute for Advanced Study, School of Natural Sciences, Princeton, NJ 08540
AND
DONALD P. SCHNEIDER
Department of Astronomy and Astrophysics, The Pennsylvania State University, University Park, PA 16802
Received 1996 August 21; accepted 1996 November 8

ABSTRACT

Observations with the Wide-Field Camera of the *Hubble Space Telescope* (*HST*) are presented for a representative sample of 20 intrinsically luminous quasars with redshifts smaller than 0.30. These observations show that luminous quasars occur in diverse environments that include ellipticals as bright as the brightest cluster galaxies (two), apparently normal ellipticals (10), apparently normal spirals with H II regions (three), complex systems of gravitationally interacting components (three), and faint surrounding nebulosity (two). The quasar host galaxies are centered on the quasar to the accuracy of our measurements, 400 pc. There are more radio-quiet quasars in galaxies that appear to be ellipticals (seven) than in spiral hosts (three), contrary to expectations. However, three, and possibly five, of the six radio-loud quasars have detectable elliptical hosts, in agreement with expectations. The luminous quasars studied in this paper occur preferentially in luminous galaxies. The average absolute magnitude of the hosts is 2.2 mag brighter than expected for a field galaxy luminosity function.

The superb optical characteristics of the repaired *HST* make possible the detection of close galactic companions; we detect eight companion galaxies within projected distances of 10 kpc from quasar nuclei. The presence of very close companions, the images of current gravitational interactions, and the higher density of galaxies around the quasars suggest that gravitational interactions play an important role in triggering the quasar phenomenon.

Subject headings: galaxies: clusters: general — galaxies: interactions — galaxies: structure — quasars: general

1. INTRODUCTION

Figures 1 and 2 (Plates 25–28) tell the main story of this paper. We urge the reader to look at these beautiful *HST* images before continuing with the text and the quantitative details.

We summarize in this paper the results of our analysis of *HST*-WFPC2 observations of a representative sample of 20 of the most luminous ($M_V < -22.9$) nearby ($z < 0.30$) quasars. The goal of these observations was to help understand the quasar phenomenon by determining the environment in which quasars occur. The main result of this paper is that there is not one type of environment but instead a wide range of environments in which the most luminous quasars appear to be embedded. The *HST* images also contain a number of extraordinary phenomena and some surprises, including very close companions, host ellipticals for radio-quiet quasars, spiral hosts with well-developed arms and prominent H II regions, galaxies caught in the act of merging, apparently faint galactic hosts, and very extended emission.

Some partial results of this study have been reported previously: Bahcall, Kirhakos, & Schneider (1994, hereafter Paper I; 1995a, hereafter Paper II; 1995b, hereafter Paper III; 1995c), Bahcall et al. (1995d, hereafter Paper IV), and Bahcall, Kirhakos, & Schneider (1996). For those aspects of the work that depend upon the subtraction of a stellar point-spread function (PSF), there are small, quantitative differences between the results described in this paper and previous results we have reported. In the previous work, we used a stellar PSF determined from a red standard star, F141. In the present work, we have used stellar PSFs that were obtained for four separate blue stars (see the discussion in § 4 of the PSFs constructed by Krist & Burrows 1996). The visual appearance of the hosts in the subtracted images is, in a few cases, significantly improved by using the PSFs of the blue stars.

Other *HST* studies of quasar imaging (although many of the objects do not satisfy our luminosity criterion) include Hutchings & Morris (1995), Hutchings et al. (1994), and Disney et al. (1995).

The subject of quasar environments has a long and distinguished history. Some representative papers that report on ground-based observations are Kristian (1973), Wyckoff et al. (1980), Wyckoff, Wehinger, & Gehren (1981), Tyson, Baum, & Kreidl (1982), Hutchings et al. (1982), Gehren et al. (1984), Heckman et al. (1984), Malkan (1984), Malkan, Margon, & Chanan (1984), Boroson, Persson, & Oke (1985), Smith et al. (1986), Hutchings (1987), Stockton & MacKenty (1987), Yee (1987), Hutchings, Janson, & Neff (1989), Romanishin & Hintzen (1989), Véron-Cetty & Woltjer (1990), Hutchings & Neff (1992), Dunlop et al. (1993), and McLeod & Rieke (1994a, 1994b).

The analyses described in these pioneering ground-based studies are made difficult because of atmospheric seeing; the light from the bright central (nuclear) sources may be a few magnitudes brighter than the total emission from the host galaxies. Nevertheless, there is agreement (within typically 1

[1] Based on observations with the NASA/ESA *Hubble Space Telescope*, obtained at the Space Telescope Science Institute, which is operated by the Association of Universities for Research in Astronomy, Inc., under NASA contract NAS 5-26555.

mag or better) between our *HST* observations and previous ground-based estimates of the total apparent magnitudes of the host emission, although *HST* reveals details not previously accessible and corrects some important conjectures that are not supported by the higher resolution observations.

The paper is organized as follows. In § 2, we describe the sample selection and observations; in § 3, we present the unprocessed data; in § 4, we describe the method of removing the light due to the quasar (PSF subtraction) and present the data after a stellar PSF is subtracted; in § 5, we describe the methods of analysis of the data; in § 6, we report on the measurements of the host galaxies; in § 7, we discuss the presence of companion galaxies; in § 8, we compare our measurements with results from some ground-based observations; in § 9, we comment on the environment and host galaxy of each quasar; and in § 10, we summarize and discuss our results. We assume in this paper that $H_0 = 100\ \mathrm{km\ s^{-1}\ Mpc^{-1}}$ and $\Omega_0 = 1.0$.

2. SAMPLE SELECTION AND OBSERVATIONS

We describe in this section how the sample was selected (§ 2.1) and how the observations were performed (§ 2.2).

2.1. *Sample Selection*

A sample of 14 quasars was selected solely on the basis of luminosity ($M_V < -22.9$), redshift ($z \leq 0.20$), and galactic latitude ($|b| > 35°$). All the quasars in the Véron-Cetty & Véron (1991) catalog that satisfied the redshift, luminosity, and galactic latitude criteria were included in this sample; no distinction was made on the basis of radio or other secondary properties. One may choose to call this set of quasars a "complete sample" within the context of the Véron-Cetty & Véron (1991) catalog.[2]

The 14 quasars with $z \leq 0.20$ have an average (median) absolute magnitude $\langle M_V \rangle = -23.4$ (23.2) and an average redshift $\langle z \rangle = 0.17$. Only three radio-loud quasars are present in the original sample of 14 objects. In the Véron-Cetty & Véron (1996) catalog, there are an additional four quasars with $z \leq 0.20$ that satisfy our luminosity and galactic latitude requirements; all are radio quiet.

By combining the time available from GTO and GO programs, an additional six quasars with redshifts in the range $0.20 < z < 0.30$ were added to the original sample of 14 objects; these additional objects satisfied the same luminosity and galactic latitude constraints as the original sample. The additional objects contain three radio-loud quasars; the total sample of 20 contains six quasars that are classified as radio loud, i.e., with $L_{5\ \mathrm{GHz}} \gtrsim 10^{26}\ \mathrm{W\ Hz^{-1}}$ (Kellermann et al. 1994). The additional six objects are slightly brighter in the optical on the average (median), $\langle M_V \rangle = -24.0$ (-24.1), and have slightly larger redshifts, $\langle z \rangle = 0.26$. The range of absolute magnitudes in the six added objects, $-24.6 \leq M_V < -22.9$, is included within the range of absolute magnitudes spanned by the original sample of 14 objects, i.e., $-25.6 \leq M_V < -22.9$.

[2] The concept of a "complete" sample of quasars requires clarification since a variety of techniques, including radio emission, optical colors, variability, and X-ray emission, are used to discover quasars. It is conceivable, indeed likely, that there is at least one object satisfying our defining sample criteria that has not yet (in 1996) been recognized observationally. For lack of a better term, we use here the designation "complete sample" in a limited sense to mean all the objects within a specified catalog having stated characteristics.

In what follows, we shall refer to the total sample of 20 quasars as a "representative sample" with $M_V < -22.9$ and $z < 0.30$. The average (median) absolute magnitude for the full sample is -23.6 (-23.2); the average redshift $\langle z \rangle = 0.19$. Nearly all (18) of the quasars have $15.1 < V < 16.7$, but two are much brighter in the optical band: 3C 273 ($V = 12.8$) and HE 1029−140 ($V = 13.9$).

2.2. *Observations*

A journal of the observations is given in Table 1, which lists the following quantities for each object: the date observed, the longest exposure time of a single image, the detected number of electrons $\mathrm{pixel^{-1}\ s^{-1}}$ in the sky, the quasar redshift, the distance in kiloparsecs that corresponds to an angular separation of 1″ as seen from Earth, the apparent V magnitude (from Véron-Cetty & Véron 1996), the absolute V magnitude (without k-correction), the radio properties (an X identifies the radio-loud quasars), and in the last column the existence of *HST* spectroscopy (a "K" indicates that the *HST*/FOS observations were taken as part of the *HST* Quasar Absorption Line Key Project, and some of the results are reported by Bahcall et al. 1993 and Jannuzi et al. 1997); an "O" indicates that other FOS observations exist).

The quasars were observed with the Wide Field/Planetary Camera-2 (WFPC2) through the F606W filter, which is similar to the V bandpass but is slightly redder; the mean wavelength and FWHM of the F606W system response are 5935 and 1500 Å, respectively. The F606W filter was chosen because of its high throughput. In all of the quasars discussed here, redshifted Hβ and [O III] are included in the bandpass. At a given angular radius, the scattered light in the Wide Field Camera-2 (WF) is about 5 times less than the scattered light in the Planetary Camera (see Krist & Burrows 1994). We chose to use the WF instead of the PC in the original formulation of this program because of the likelihood that the host galaxies would have low surface brightnesses that extended over areas large compared to the WF resolution (0.″1 or about 0.2 kpc). The results reported here support the original choices, since the observed galaxy extensions are indeed large compared to the WF resolution.

The center of light of all quasars was placed within $4'' \pm 1''$ from the center of the Wide-Field Camera CCD 3 (WF3). Three exposures were taken of each quasar. The integration times for 14 objects were 1400, 500, and 200 s; the exposures for the remaining six objects were 1100, 600, and 100 s.

The size of WF3 is 800×800 pixels (exposed area $\sim 770 \times 750$ pixels), and its image scale is 0.″0996 $\mathrm{pixel^{-1}}$. We report measured F606W magnitudes on the *HST* photometric scale established by Holtzman et al. (1995b). The adopted photometric zero point for 1 electron $\mathrm{s^{-1}}$ is 24.94 mag for the F606W filter. For further information about the WFPC2, see Burrows (1994), Trauger et al. (1994), and Holtzman et al. (1995a, 1995b). Additional details of the observational procedures are given in Paper I and Paper II.

The innermost regions of the quasar images are saturated in all of the longest exposures out to a radius ≈0.″3, except for the two optically brightest quasars in our sample, HE 1029−140 and 3C 273, in which cases the images were saturated out to ≈0.″5 and 0.″7, respectively. The number of saturated pixels in the central region of the quasar images were typically 30 pixels for the longest exposures. In addi-

TABLE 1

QUASAR SAMPLE

Object	Date	Time (s)	Sky Level (e^- pixel^{-1} s^{-1})	z	kpc arcsec^{-1}	V	M_V(QSO)[a]	Radio-loud	FOS[b]
PG 0052+251	1994 Dec 5	1400	0.114	0.155	1.75	15.4	−23.0		
PHL 909	1994 Oct 17	1400	0.136	0.171	1.88	15.7	−22.9		
NAB 0205+02	1994 Oct 26	1400	0.139	0.155	1.75	15.4	−23.0		
0316−346	1994 Nov 20	1400	0.075	0.265	2.55	15.1	−24.5		
PG 0923+201	1995 Mar 23	1400	0.136	0.190	2.04	15.8	−23.1		
PG 0953+414	1994 Feb 3	1100	0.110	0.239	2.38	15.3	−24.1		K
PKS 1004+130.....	1995 Feb 26	1400	0.150	0.240	2.39	15.2	−24.2	X	
PG 1012+008	1995 Feb 25	1400	0.129	0.185	2.00	15.6	−23.2		
HE 1029−140	1995 Feb 6	1400	0.100	0.086	1.22	13.9	−23.2		
PG 1116+215	1994 Feb 8	1100	0.128	0.177	1.93	14.7	−24.0		K, O
PG 1202+281	1994 Feb 8	1100	0.116	0.165	1.83	15.6	−23.0		K
3C 273	1994 Jun 5	1100	0.151	0.158	1.78	12.9	−25.6	X	K, O
PKS 1302−102.....	1994 Jun 9	1100	0.136	0.286	2.67	15.2	−24.6	X	K
PG 1307+085	1994 Apr 5	1400	0.129	0.155	1.75	15.1	−23.3		
PG 1309+355	1995 Mar 26	1400	0.088	0.184	1.99	15.6	−23.2		O
PG 1402+261	1995 Mar 7	1400	0.089	0.164	2.13	15.5	−23.0		
PG 1444+407	1994 Jun 27	1100	0.071	0.267	2.56	15.7	−23.9		K, O
3C 323.1	1994 Jun 9	1100	0.082	0.266	2.55	16.7	−22.9	X	
PKS 2135−147.....	1994 Aug 15	1400	0.174	0.200	2.11	15.5	−23.5	X	O
PKS 2349−014.....	1994 Sep 18	1400	0.161	0.173	1.90	15.3	−23.4	X	

[a] Computed for $\Omega_0 = 1.0$ and $H_0 = 100$ km s^{-1} Mpc^{-1}. In this cosmology, brightest cluster galaxies have $M_V \approx -22.0$ (Hoessel & Schneider 1985; Postman & Lauer 1995) and the characteristic (Schechter-) magnitude for field galaxies is $M_V^* = -20.5$ (Schechter 1976; Kirshner et al. 1983; Efstathiou, Ellis, & Peterson 1988).

[b] K = *HST* Quasar Absorption Line Key Project; O = Other FOS observations.

tion, ~15 saturated pixels were present due to the "vertical bleeding." For HE 1029−140 and 3C 273, the number of saturated pixels was approximately 105 and 190, respectively, plus 90 and 390 from the vertical bleeding (see Fig. 1).

The initial data processing (bias frame removal and flat-field calibration) was performed at the Space Telescope Science Institute with their standard software package. The individual images of each quasar were aligned to better than 0.3 pixel; this made it easy to identify and eliminate cosmic-ray events. Cosmic rays were identified by a pixel-by-pixel comparison of pairs of images; the intensity of a pixel containing a cosmic ray was replaced by the scaled value of the intensity of the pixel in the other image. The flat-field corrections were based upon preflight calibrations; these calibrations remove the small-scale (few pixel) sensitivity variations. The typical signal and rms of the noise of the sky in the long exposures (in detected photons per pixel) are 157 and 14, respectively.

The sky level corresponds to an average surface brightness of approximately 22.2 mag arcsec^{-2}. The limiting surface brightness at which objects can be detected is typically between 25 and 26 mag arcsec^{-2} (F606W); see Table 2.

3. THE UNPROCESSED IMAGES

We present in this section the images as received from STScI, without further processing except for the removal of cosmic rays.

Figure 1 shows a 23″ × 23″ WF image of each of the 20 quasars, plus the image of a blue star (*upper left-hand panel*). The images displayed are the longest individual exposures we have. Many, but not all, of the quasars are noticeably nonstellar, and host galaxies are visible on the unprocessed *HST* images. The exposure time of the star image shown in the top panel of Figure 1 is 20 s, which yields a total number of counts similar to that obtained in the quasar images. The star is MMJ 6490 in the M67 cluster. Its apparent V magnitude is 10.99, and its $B-V = 0.11$ (Montgomery, Marschall, & Janes 1993).

Some features of host galaxies are obvious in Figure 1. Normal spiral galaxies, with prominent H II regions envelop PG 0052+251 and PG 1402+261. Host elliptical galaxies are clearly seen in the images of PHL 909, HE 1029−140, PG 1116+215, and 3C 273. There are three obvious cases of current gravitational interaction: 0316−346, PG 1012+008, and PKS 2349−014.

Some of the host galaxies are seen even in our shortest exposures (200 s; see Bahcall et al. 1996 for short-exposure images of PG 0052+251 and PHL 909). In some cases, such as NAB 0205+02, PG 0953+414, and PG 1307+085, it is difficult to distinguish the quasar image from the star even in our longest exposures.

4. IMAGES AFTER SUBTRACTION OF A STELLAR PSF

The major challenge in the analysis of these *HST* data is the removal of the light produced by the quasar, which is presumed to be a point source. We have adopted an empirical approach. We have used images of stars observed at the same location on the detector as the quasars to determine the PSF of the stellar quasar.

For about half of the quasars considered here, the principal observational results concerning the host environment can be obtained without the PSF subtraction. Examples of exceptions are the hosts of NAB 0205+02, PG 0953+414, PG 1444+407, and 3C 323.1, which are more apparent in Figure 2 than in Figure 1. Close companions for PKS 1302−102, PKS 2135−147, and PKS 2349−014 are also more clearly visible after the subtraction of a stellar PSF.

The stellar PSF was measured in Cycle 5 (*HST* program 5849) by obtaining a set of 13 images for each of four blue stars in the M67 cluster. The calibration stars (and their $B-V$ colors) are MMJ 6481(−0.073), MMJ 6490(0.11), MMJ 6504(0.22), and MMJ 6511(0.34). The apparent magnitudes range from $V = 10.03$ to $V = 10.99$. For each star, a

series of four images were used by Krist & Burrows (1996) to produce a PSF that samples the full dynamic range of the star image and covers the saturation range found in the quasar images. In these calibration images, the radius of the saturated region varies from 0".0 to 0".6; the exposure times range from 0.1 to 100 s.

The PSF data are publicly available at http://www.sns.ias.edu/jnb. There is a detailed documentation regarding the PSF data and their use at this site (go to HST Images) by J. Krist and C. Burrows describing how the PSFs were constructed.

Whenever PSF subtractions were required, we used all four PSFs determined by Krist and Burrows. For each case, we selected the result that gave the cleanest subtraction (i.e., the fewest artifacts produced).

We fitted a stellar PSF to each quasar image and subtracted a multiple of the normalized PSF to search for underlying diffuse light from hosts. The best fit was determined by minimizing the differences between the quasar and the PSF using a χ^2-routine calculated in two distinct areas: azimuthal averages and narrow regions centered on the diffraction spikes. The two methods gave essentially same results (see Paper II), differing in inferred host galaxy magnitude by ± 0.1 mag. The quasar images with the PSF subtracted presented in this paper were obtained by minimizing the χ^2 in unsaturated annular region (typical inner and outer radii of 1" and 3"), centered on the quasar. Adjustments of the amount of PSF subtraction were often made after visual inspection of the "best-fit" PSF-subtracted images.

We have estimated some of the likely systematic uncertainties in the subtraction process by subtracting a best-fit PSF of the standard star, MMJ 6504, from the image of another standard star, MMJ 6490. We have Cycle 5 observations of MMJ 6490 observed at the same position in WF3 as the sample quasars. Figure 2 (*upper left-hand panel*) shows the image of the best fit of MMJ 6504 subtracted from MMJ 6490. The PSF subtraction, star from star, is very good, although some faint diffuse residuals are still present. If we scale the intensity of MMJ 6490 so that the central brightness corresponds to the apparent magnitude of one of our typical quasars, i.e., $V = 15.6$, then the residual "nebulosity" left over when the MMJ 6504 PSF is subtracted is about 21.0 mag.

Figure 2 shows the images for all the quasars in our sample after a best-fit stellar PSF was subtracted from the original images shown in Figure 1.

Table 2 lists the major diameter of the host galaxies in arcseconds and in kiloparsecs, the surface brightness of the isophote for which the size was measured, and a tentative morphological classification. For each quasar, the magnitude of the host galaxy was calculated using three different methods, aperture photometry (see § 5.1), and one-dimensional and two-dimensional galaxy modeling (see §§ 5.2 and 5.3).

We determined the size of the quasar hosts by examining the PSF-subtracted images and measuring the faintest isophotes of the host galaxy. The morphological classification was done by visual inspection of the images and following as closely as possible the classification given in The Hubble Atlas of Galaxies by Sandage (1961). In a number of cases indicated by (?) in Table 2, we have denoted as "En" featureless, smooth hosts that do not show any obvious discontinuities or morphological features.

5. METHODS OF ANALYSIS

In this section, we describe the different methods of analysis that we have used to determine the properties of the quasar hosts. The measured quantities are presented in Tables 2–6 and discussed in §§ 6–7. We describe in §§ 5.1 –5.3 different methods for estimating the magnitude of the host galaxies. We discuss in § 5.1 our results for aperture photometry, in § 5.2 the radial profile fits, and in § 5.3 the two-dimensional fits.

Some of the host environments are complex, including merging or tidally interacting galaxies and close companions. The smooth de Vaucouleurs or exponential disk models used in §§ 5.2 and 5.3 are obviously not realistic descriptions of the light distribution for complex environments. In order to provide a common basis of comparison

TABLE 2

SIZE AND MORPHOLOGY OF HOST GALAXIES

OBJECT	MAJOR DIAMETER arcsec	MAJOR DIAMETER kpc	ISOPHOTE (F606W) (mag arcsec^{-2})	MORPHOLOGY
PG 0052+251	20	35	25.1	Sb
PHL 909	19	36	24.7	E4
NAB 0205+02	9	16	25.0	S0?
0316−346	17	43	25.6	Complex, interaction
PG 0923+201	13	27	24.8	E1
PG 0953+414	11	26	25.8	Faint, tail?
PKS 1004+130.....	15	36	25.0	E2
PG 1012+008	18	36	25.0	Interacting galaxies
HE 1029−140	40	49	26.0	E1
PG 1116+215	14	27	25.1	E2
PG 1202+281	10	18	24.7	E1, bright companion
3C 273	29	52	25.4	E4
PKS 1302−102.....	15	40	25.2	E4 (?) two close companions
PG 1307+085	9	16	24.6	Faint E1 (?)
PG 1309+355	18	36	25.7	Sab
PG 1402+261	14	30	25.6	SBb
PG 1444+407	10	26	25.2	E1 (?)
3C 323.1	11	28	25.1	E3 (?) (bright companion)
PKS 2135−147.....	15	32	24.8	E1 (companions)
PKS 2349−014.....	21	40	24.5	Complex, interacting

with ground-based observations, we provide the results of fits with smooth models for all of the host environments, complex or not.

5.1. *Aperture Photometry*

We performed aperture photometry in circular annuli centered on the quasars, after a best-fit PSF was subtracted. An inner radius of $r = 1''.0$ was used for all quasars, except for HE 1029−140 and 3C 273. In most observations, the region $r < 1''$ is heavily contaminated by artifacts left by the PSF subtraction. The saturated areas in the images of HE 1029−140 and 3C 273 are larger; for those two cases, the inner radii used were $1''.5$ and $2''.0$, respectively. The outer radii chosen in general represent how far we could see the host galaxy (see Table 3). The aperture magnitudes calculated using an inner radius $r = 1''.0$ are typically ~ 0.6 mag fainter than the total magnitude for the galaxy that was estimated by fitting a model (see §§ 5.2–5.3) to the measured surface brightness. A difference between aperture and model magnitudes is expected because the aperture magnitudes do not include the area within $1''$ of the quasar; all of the models we considered have surface brightnesses that increase monotonically toward the center.

5.2. *One-dimensional Radial Profiles*

The one-dimensional azimuthally averaged surface brightness profiles of the host galaxies were constructed from the *HST* data after subtraction of a best-fit stellar PSF. Regions affected by saturation, diffraction spikes, or residual artifacts from the PSF subtraction were not included in the azimuthally averaged profiles. For each galaxy, we obtained a best-fitting exponential disk (hereafter Disk) and a de Vaucouleurs (1948, hereafter GdV) profile that fits the observed data in the region $r \geq 1''$. The total magnitudes obtained this way are systematically brighter than the ones obtained by aperture photometry (§ 5.1), which excludes the innermost, saturated regions of the profiles.

5.3. *Two-dimensional Fit*

The *HST* imaging provides greater detail than has been available previously in ground-based images of luminous quasars. Traditionally, the properties of host galaxies have been determined in ground-based studies by making model fits to azimuthally averaged radial profiles (see § 5.2).

To take advantage of the *HST* resolution, we have developed software to fit a two-dimensional model to the PSF-subtracted quasar images. For each quasar, we fitted an analytic galaxy model (exponential disk or de Vaucouleurs profile) to the data and calculated the χ^2. The area used for the fit was approximately an annular region, centered on the quasar, that excluded the central area ($r < 1''.0$), and the remnants of the diffraction spikes or other artifacts clearly due to improper PSF subtraction. We fitted four parameters: the (x, y) pixel position of the center, the total number of counts, and the radius (effective radius or scale length) in the galaxy model.

We begin the iteration by giving the software the position of the quasar nucleus and calculate only the total number of counts. The number of counts found in this step is entered as the initial guess for the galaxy brightness, and the program then fits the counts and radius, keeping the position fixed. Finally, we supply the software with the previously calculated counts and radius and ask the software to fit all four parameters.

We tested the software for the two-dimensional fits in different ways. Initially, we created two model galaxies: a disk and an elliptical galaxy. We checked how well the two-dimensional software reproduced the position of the center of the model galaxies, the scale length or effective radius, and the total number of counts. We made extensive checks by varying the input parameters and the order in which the parameters were fitted. The best results were achieved when we followed the three-step iterative process in the order described above. We fitted each model galaxy with an exponential disk and a de Vaucouleurs model—the smallest χ^2 residuals were obtained when the disk galaxy was fitted by an exponential disk model and the elliptical was fitted by a de Vaucouleurs model. For the model galaxies, the discrepancy in position and size were <1 pixel. The discrepancy in the total number of counts was $\sim 1\%$. The accuracy achieved in the simulations is greater than can be achieved with the real data because of the imperfect subtraction of the PSF for the *HST* images.

The host galaxies of PG 0052+251 and PHL 909 were also used to test the two-dimensional software. We compared the software output position with our measured position for the center of the galaxy (agreement better than $0''.2$), compared the total number of counts with the value we estimated from aperture photometry (agreement turned out to be 0.1 mag for PG 0052+251, and 0.5 mag for PHL 909), and verified that the output scale length or effective radius were plausible.

6. MAGNITUDES AND POSITIONS OF HOST GALAXIES

In this section, we report on the measurements of the magnitude and position of the host galaxies.

In Table 3, we list the magnitudes for the host galaxies measured using aperture photometry; the inner and outer radii used in performing aperture photometry are listed as well. The outer radius indicates how far from the quasar the host galaxy was clearly visible. We transformed the measured F606W aperture magnitudes to V applying k-corrections calculated by Fukugita, Shimasaku, & Ichikawa (1995). Given the redshift of the quasar and the morphological type of the host, we used Table 6 and Figure 14*b* of Fukugita et al. to obtain the (F606W − V) color. For the cases in which we are uncertain about the morphological type of the host, we assumed an average of the (F606W − V) color for ellipticals and Sab galaxies.

Table 4 lists the results for the one-dimensional and two-dimensional galaxy model fitting. The two-dimensional models are somewhat fainter than the corresponding one-dimensional fits. Specially, we find

$$\langle m_{606\mathrm{W},2\text{-D}} - m_{606\mathrm{W},1\text{-D}} \rangle = \begin{cases} 0.4 \pm 0.2\,, & \mathrm{GdV} \\ 0.3 \pm 0.1\,, & \mathrm{Disk} \end{cases} . \quad (1)$$

The magnitudes obtained by model fits are brighter than those obtained by aperture photometry since the models include estimated contributions from the inner (saturated) regions of the images. On average,

$$\langle m_{606\mathrm{W},1\text{-D}} - m_{606\mathrm{W},\mathrm{aperture}} \rangle = \begin{cases} -1.1 \pm 0.2\,, & \mathrm{GdV} \\ -0.4 \pm 0.2\,, & \mathrm{Disk} \end{cases} . \quad (2)$$

As equation (3) shows, the magnitudes of the host galaxies estimated by fitting a GdV model to the azimuthal averaged

TABLE 3

APERTURE MAGNITUDES FOR HOST GALAXIES

OBJECT	INNER RADIUS (arcsec)	OUTER RADIUS (arcsec)	APERTURE PHOTOMETRY m_{F606}	APERTURE PHOTOMETRY M_{F606}	(F606 − V)[a]	APERTURE PHOTOMETRY M_V
PG 0052+251	1.0	10.0	17.1	−21.3	−0.31	−21.0
PHL 909	1.0	10.0	17.5	−21.1	−0.41	−20.7
NAB 0205+02	1.0	4.5	19.5	−18.9	−0.31	−18.6
0316−346	1.0	11.5	18.2	−21.4	−0.47	−20.9
PG 0923+201	1.0	6.5	18.3	−20.6	−0.42	−20.2
PG 0953+414	1.0	5.5	19.1	−20.3	−0.38	−19.9
PKS 1004+130.....	1.0	7.5	17.7	−21.7	−0.48	−21.2
PG 1012+008	1.0	4.5	17.8	−21.0	−0.39	−20.6
HE 1029−140	1.5	20.0	16.5	−20.6	−0.35	−20.2
PG 1116+215	1.0	8.0	17.7	−21.0	−0.41	−20.6
PG 1202+281	1.0	5.0	18.6	−20.0	−0.40	−19.6
3C 273	2.0	15.0	16.6	−21.9	−0.40	−21.5
PKS 1302−102.....	1.0	7.5	18.4	−21.4	−0.50	−20.9
PG 1307+085	1.0	4.5	18.7	−19.7	−0.37	−19.3
PG 1309+355	1.0	9.0	17.4	−21.4	−0.35	−21.0
PG 1402+261	1.0	7.5	18.1	−20.4	−0.30	−20.1
PG 1444+407	1.0	5.0	18.8	−20.8	−0.47	−20.3
3C 323.1	1.0	5.5	18.9	−20.7	−0.47	−20.2
PKS 2135−147.....	1.0	7.5	18.1	−20.9	−0.45	−20.4
PKS 2349−014.....	1.0	12.0	16.7	−22.0	−0.41	−21.6

[a] Fukugita et al. 1995.

radial profile of the residual light are on average 1.0 mag brighter than the magnitudes obtained from aperture photometry; fitting an exponential disk model gives magnitudes that are on average 0.5 brighter than the results from aperture photometry. For the two-dimensional model fits, we have on average

$$\langle | m_{606W,2\text{-}D} - m_{606W,aperture} | \rangle = \begin{cases} -0.7 \pm 0.2\,, & \text{GdV} \\ -0.2 \pm 0.1\,, & \text{Disk} \end{cases} . \quad (3)$$

Table 5 lists our best estimate absolute V magnitudes. In computing the entries in Table 5, we used the k-correction values of Fukugita et al. (1995) that are listed in the next-to-last column of Table 3. In computing the absolute magnitudes, we selected the best-fit model based on the morphology of the host galaxy, unless the morphology is uncertain, and for those cases, we list the model that gives the smallest χ^2 residuals.

The results from the two-dimensional fits indicate that the host galaxies are, on average, centered on the quasar with

$$\langle \Delta r \rangle = 0.4 \pm 0.4 \text{ kpc} . \quad (4)$$

The host galaxies are typically centered within 400 pc of the location of the quasar point source. If we eliminate from the

TABLE 4

MODEL FITS TO STELLAR QUASAR PLUS HOST GALAXY

	ONE-DIMENSIONAL				TWO-DIMENSIONAL			
	GdV		Exponential Disk		GdV		Exponential Disk	
OBJECT	m_{F606}	r(arcsec)[a]	m_{F606}	r(arcsec)[b]	m_{F606}	r(arcsec)[a]	m_{F606}	r(arcsec)[b]
PG 0052+251	16.1	4.7	16.8	1.4	16.7	1.8	17.2	1.3
PHL 909	16.7	2.5	17.4	1.0	17.2	2.3	17.6	1.5
NAB 0205+02	18.0	0.6	18.7	0.6	18.4	0.7	19.0	0.7
0316−346	17.2	3.4	18.0	1.1	17.8	2.1	18.3	1.2
PG 0923+201	17.3	2.5	18.0	1.0	17.5	2.9	18.2	1.3
PG 0953+414	17.9	2.3	18.5	1.1	18.2	1.8	18.8	1.1
PKS 1004+130.....	16.7	1.6	17.3	0.9	16.9	1.2	17.5	1.0
PG 1012+008	16.3	6.2	17.3	1.4	17.0	3.4	17.7	1.6
HE 1029−140	15.9	2.8	16.4	1.5	16.2	3.2	16.7	1.9
PG 1116+215	16.6	1.9	17.3	1.0	16.9	1.4	17.5	1.2
PG 1202+281	17.4	1.5	18.1	0.9	17.7	1.4	18.3	1.0
3C 273	15.6	2.3	16.2	1.3	16.0	3.7	16.7	1.6
PKS 1302−102.....	17.1	2.6	17.8	1.1	17.7	1.4	18.2	1.1
PG 1307+085	17.4	1.8	18.1	0.9	17.8	1.3	18.4	1.0
PG 1309+355	16.4	2.8	17.1	1.1	16.8	2.0	17.3	1.2
PG 1402+261	16.9	2.2	17.6	1.0	17.6	1.5	18.3	1.6
PG 1444+407	17.6	1.3	18.2	1.0	17.8	1.3	18.4	1.0
3C 323.1	17.8	1.4	18.4	0.9	18.1	1.6	18.7	1.0
PKS 2135−147.....	17.2	2.0	17.8	1.1	17.4	2.6	18.0	1.3
PKS 2349−014.....	15.9	5.6	16.6	1.6	16.2	4.8	16.8	2.5

[a] Effective radius.
[b] Exponential scale length.

TABLE 5

ABSOLUTE VISUAL MAGNITUDES FOR QUASAR HOST GALAXIES

	ONE-DIMENSIONAL		TWO-DIMENSIONAL	
OBJECT	M_V(1-D)	Best Model	M_V(2-D)	Best Model
PG 0052+251	−21.3	Disk	−20.9	Disk
PHL 909	−21.5	GdV	−21.0	GdV
NAB 0205+02	−19.4	Disk	−19.1	Disk
0316−346	−21.1	Disk	−20.8	Disk
PG 0923+201	−21.2	GdV	−21.0	GdV
PG 0953+414	−20.5	Disk	−20.2	Disk
PKS 1004+130.....	−22.5	GdV	−22.0	GdV
PG 1012+008	−22.1	GdV	−20.7	Disk
HE 1029−140	−20.8	GdV	−20.5	GdV
PG 1116+215	−21.7	GdV	−21.4	GdV
PG 1202+281	−20.8	GdV	−20.5	GdV
3C 273	−22.5	GdV	−22.1	GdV
PKS 1302−102.....	−21.5	Disk	−21.1	Disk
PG 1307+085	−20.6	GdV	−20.2	Disk
PG 1309+355	−21.3	Disk	−21.1	Disk
PG 1402+261	−20.6	Disk	−19.9	Disk
PG 1444+407	−20.9	Disk	−20.5	Disk
3C 323.1	−21.3	GdV	−21.0	GdV
PKS 2135−147.....	−21.3	GdV	−21.1	GdV
PKS 2349−014.....	−22.4	GdV	−22.1	GdV

comparison the most extreme examples of especially complex environments (0316−346, PG 1012+008, and PKS 2349−014) the results are

$$\langle \Delta r \rangle = 0.2 \pm 0.2 \text{ kpc} . \quad (5)$$

The two-dimensional (one-dimensional) GdV model gives magnitudes for the host that are on average 0.6 mag (0.7 mag) brighter than the exponential disk estimates.

7. COMPANION GALAXIES

Inspection of the *HST* images of the quasar fields reveals a number of companion galaxies projected close to the quasars. The relatively long exposures (1100 or 1400 s), combined with the excellent angular resolution, allowed galaxies to be identified down to limiting magnitude m(F606W) $\lesssim$ 25.0 and as close as 1″ or 2″ from the central quasar. We performed aperture photometry on the galaxies in the quasar fields using circular apertures with radii of 0.″3–10″, as appropriate.

We counted the number of companion galaxies brighter than a specified limiting absolute magnitude that were found to have a metric separation from one of the quasars of less than or equal to some predetermined distance. We choose a priori a limiting absolute magnitude of $M_V = -16.5$ (4 mag fainter than L^*) and a maximum separation of 25 kpc (see Paper II).

Table 6 lists all galaxies found around the quasars that satisfy these specifications. This table gives for each quasar the number of companion galaxies that are at least as bright as $M_V = -16.5$ (if they have the same redshift as the quasar) and that are projected within 25 kpc of the center of light of the quasar. The separations both in arcseconds and in kpc are also given in Table 6, along with the brightnesses of the companion galaxies, tabulated in both apparent and absolute magnitude.

The density of companion galaxies brighter than $M_V = -16.5$, within 25 kpc of the quasars, may be higher around quasars with elliptical hosts. There are two companions for four spiral hosts and 13 companions for 12 elliptical hosts.

Fisher et al. (1996) examined the clustering of galaxies around all the quasars in this sample and found a significant enhancement of galaxies within a projected separation of $\lesssim 100\ h^{-1}$ kpc of the quasars. Modeling the quasar/galaxy correlation function as a power law with a slope given by the galaxy/galaxy correlation function, Fisher et al. (1996) find that the ratio of the quasar/galaxy to galaxy/galaxy correlation functions is 3.8 ± 0.8. The galaxy counts within $r < 15\ h^{-1}$ kpc of the quasars are too high for the density profile to have an appreciable core radius ($\gtrsim$100

TABLE 6

GALAXY COMPANIONS BRIGHTER THAN $M_{(F606W)} = -16.5$ WITHIN 25 kpc OF THE QUASAR

		DISTANCES		MAGNITUDES	
QUASAR	NUMBER OF COMPANIONS	arcseconds	kpc	m_{F606}	M_{F606}
PG 0052+251	1	14.1	24.6	18.8	−19.6
PHL 909	1	12.5	23.5	21.4	−17.2
NAB 0205+02	1	8.3	14.5	20.0	−18.4
PG 0923+201	2	10.9	22.2	19.5	−19.4
		11.0	22.5	18.0	−20.9
PG 0953+414	1	8.2	19.6	22.7	−16.7
PG 1012+00	2	3.3	6.7	17.6	−21.2
		6.8	13.7	19.0	−19.8
PG 1116+215	1	12.3	23.8	19.3	−19.4
PG 1202+281	3	5.2	9.5	18.9	−19.7
		8.4	15.3	21.5	−17.1
		9.6	17.5	21.3	−17.3
PKS 1302−102.....	2	1.1	2.9	20.3	−19.5
		2.3	6.2	21.5	−18.3
HE 1029+140[a]	1	4.1	5.0	20.7	−16.4
3C 323.1	1	2.7	6.9	20.6	−19.0
PKS 2135−147.....	2	1.9	3.9	19.5	−19.5
		5.5	11.7	19.7	−19.3
PKS 2349−014.....	2	1.9	3.5	20.8	−17.9
		11.6	22.0	21.4	−17.3

[a] Absolute magnitude of the close companion is 0.1 mag fainter than the assumed limiting magnitude.

h^{-1} kpc). These results provide further support for the idea that low-redshift quasars are located preferentially in groups of 10–20 galaxies rather than in rich clusters. Fisher et al. do not detect a significant difference in the clustering amplitudes derived from radio loud and radio quiet subsamples.

8. COMPARISON WITH GROUND-BASED OBSERVATIONS

In this section we compare the results of *HST*-based images of luminous quasars with previously published representative analyses of ground-based observations. In § 8.1, we compare our *HST* measurements with the Véron-Cetty & Woltjer (1990) *i*-band results, in § 8.2, with the Dunlop et al. near-infrared images, and in § 8.3, with the McLeod & Rieke (1994b) *H*-band observations.

8.1. *Véron-Cetty & Woltjer: Annular Regions*

Véron-Cetty & Woltjer (1990) suggested that the apparent magnitudes of host galaxies should be measured in a fixed metric annulus that is well removed from the quasar nucleus. They proposed an annular region of 12.5–25.0 kpc for $\Omega_0 = 0.0$ and $H_0 = 50$ km s^{-1} Mpc^{-1}. The Véron-Cetty & Woltjer proposal compares directly measurements of the same quantity made by separate groups using different techniques. In this way, measurement uncertainties can be separated from differences caused by the variety of choices in the models used to fit to the observations.

We have three objects in common with Véron-Cetty & Woltjer: PKS 1302−102, PKS 2135−147, and PKS 2349−014. The specified annular regions are 2.″17 and 4.″35, 2.″82 and 5.″63, and 3.″15 and 6.″30 for the three quasars, respectively. All three quasars have close companion galaxies in the regions specified by Véron-Cetty & Woltjer (see Table 6). The close companions of PKS 1302−102 and PKS 2349−014 were not noticed on the ground-based images.

Table 7 summarizes the aperture photometry that was performed in the same annular regions as Véron-Cetty & Woltjer. We list the *i*-band annular magnitudes obtained by Véron-Cetty & Woltjer and their estimated absolute *V*-magnitude, converted to the cosmological parameters used in this paper, the absolute magnitude we measured in the *HST* images (excluding the light of the companions) with the F606W, and our estimated absolute *V*-magnitude. We also include in the table the total absolute *V*-magnitude Véron-Cetty & Woltjer obtained for the host galaxies (fitting a spheroidal model) and our estimated two-dimensional *V*-band host galaxy magnitude.

The agreement between our results and the ground-based observations of Véron-Cetty & Woltjer for the aperture photometry between 12.5 and 25 kpc is satisfactory but not as precise as we would have hoped. The average difference between our estimated M_V and that of Véron-Cetty & Woltjer is

$$\langle M_{V(i)} - M_{V(\mathrm{F606})} \rangle_{(12.5-25\ \mathrm{kpc})\mathrm{VCW}} = -0.4 \pm 0.1\ \mathrm{mag}\ . \quad (6)$$

This discrepancy cannot be attributed to the contribution of companion galaxies. In the case of PKS 1302−102, the companion at 2″ lies inside the annular region studied (12–25 kpc); if we include its light, our estimated brightness for the host increases 0.2 mag. Part of the companion galaxy 5.″5 from PKS 2135−147 lies in the annular region considered, but Véron-Cetty & Woltjer (1990) also subtracted its contribution from their measurements. The compact companion at 2″ of PKS 2349−014 lies outside the annular region considered.

The Véron-Cetty & Woltjer magnitudes for the host that were estimated by fitting a spheroidal model are typically about 1 mag brighter than our two-dimensional model magnitudes, i.e.,

$$\langle M_{V(i)}(\mathrm{model})_{\mathrm{VCW}} - M_{V(\mathrm{F606})}(\mathrm{2\text{-}D}) \rangle = -0.8 \pm 0.4\ \mathrm{mag}\ . \quad (7)$$

Table 8 lists the annulus measurements of the whole sample. For the range of redshifts in our sample, the designated Véron-Cetty & Woltjer annular region 12.5–25 kpc ($H_0 = 50$ km s^{-1} Mpc^{-1}, $\Omega_0 = 0.0$) corresponds approximately to 6–12 kpc with our chosen cosmological parameters. In Table 8 we list for each quasar the inner and outer radii in arcseconds, the apparent and absolute F606 aperture magnitude, and the absolute *V* magnitude in the annulus (see adopted values for F606 − *V* values in Table 3). As stressed by Véron-Cetty & Woltjer (1990), these annular measurements can be compared to future measurements obtained by other techniques.

8.2. *Dunlop et al.*

Dunlop et al. (1993) obtained deep ground-based near-infrared images in the *K* band for a sample of nearby ($z < 0.4$) radio-loud and radio-quiet quasars. They built a library of infrared PSFs by observing many bright stars. The nuclear component was removed by selecting from the library the PSF that produced the best match to the quasar PSF. The stellar PSF was scaled to the same height as the central peak of the quasar. Dunlop et al. suggest that their procedure will cause the luminosities of the hosts to be overestimated, but in practice the sign of the error could depend on whether there was a positive or a negative fluctuation in the measured light in the central peak. An aperture diameter of 12″ was used by Dunlop et al. to measure

TABLE 7

COMPARISON WITH RESULTS OF VÉRON-CETTY & WOLTJER (1990)

	12.5 kpc–25 kpc					
OBJECT	m_i[a]	$M_{V(i)}$[a]	M_{F606}[b]	$M_{V(\mathrm{F606})}$[b]	M_V(model)[a]	$M_{V(\mathrm{F606})}$(2-D)[b]
PKS 1302−102.....	19.5	−20.3	−20.4	−20.0	−22.0	−21.1
PKS 2135−147.....	18.9	−19.9	−19.9	−19.4	−22.2	−21.1
PKS 2349−014.....	17.6	−20.7	−20.8	−20.4	−22.5	−22.1

[a] Véron-Cetty & Woltjer 1990.
[b] *HST* results, this paper.

TABLE 8

ANNULAR MAGNITUDES

Object	r_1 (arcsec)[a]	r_2 (arcsec)[b]	m_{F606}	M_{F606}	M_V
PG 0052+251	3.43	6.86	18.3	−20.1	− 19.8
PHL 909	3.19	6.38	18.8	−19.8	− 19.4
NAB 0205+02	3.43	6.86	20.7	−17.7	− 17.4
0316−346	2.80	4.71	19.8	−19.8	− 19.3
PG 0923+201	2.96	5.91	19.3	−19.6	− 19.2
PG 0953+414	2.52	5.04	20.1	−19.3	− 18.9
PKS 1004+130.....	2.51	5.02	18.9	−20.5	− 20.0
PG 1012+008	3.00	6.00	18.1	−20.7	− 20.3
HE 1029−140	5.56	11.11	18.0	−19.1	− 18.7
PG 1116+215	3.11	6.22	19.0	−19.7	− 19.3
PG 1202+281	3.28	6.56	19.9	−18.8	− 18.4
3C 273	3.37	6.74	17.8	−20.7	− 20.3
PKS 1302−102.....	2.25	4.49	19.4	−20.4	− 19.9
PG 1307+085	3.43	6.86	19.9	−18.5	− 18.1
PG 1309+355	3.02	6.03	18.7	−20.1	− 19.7
PG 1402+261	3.28	6.56	19.5	−19.0	− 18.7
PG 1444+407	2.34	4.69	19.7	−19.9	− 19.4
3C 323.1	2.35	4.71	19.9	−19.7	− 19.2
PKS 2135−147.....	2.84	5.69	19.1	−19.9	− 19.4
PKS 2349−014.....	3.16	6.32	17.9	−20.8	− 20.4

NOTE.—F606 magnitudes of host galaxies measured in an annulus between radii of 6 kpc and 12 kpc for $H_0 = 100$ km s^{-1} Mpc^{-1}, $\Omega_0 = 1.0$. (These radii corresponds approximately to 12.5 kpc and 25 kpc for $H_0 = 50$ km s^{-1} Mpc^{-1}, $\Omega_0 = 0.0$)

[a] Inner radius = 6 kpc.

[b] Outer radius = 12 kpc.

the magnitudes of the hosts. We have eight quasars in common.

Table 9 compares the *HST* and the Dunlop et al. results. We list the K magnitude they obtained for the host galaxies using an aperture of diameter 12″, the K absolute magnitude for the host, using our comoslogical parameters, the color $(V-K)$ for an elliptical galaxy obtained from Bruzual & Charlot (1993), the corresponding V absolute magnitude expected, the two-dimensional model V absolute magnitude estimated from the *HST*-F606W images (see next-to-last column of Table 5), and the difference between the V absolute magnitude derived from both bands, ΔM_V. The average discrepancy is

$$\langle\,|\Delta M_V|\,\rangle = \langle\,|M_{V(K)} - M_{V(F606)}|\,\rangle = 1.0 \pm 0.6 \text{ mag} . \quad (8)$$

For seven of the eight cases, our estimated magnitudes are brighter than obtained by Dunlop et al. (1993).

8.3. *McLeod & Rieke*

McLeod & Rieke (1994a, 1994b) obtained ground-based images of luminous quasars in the H band. For most cases, they determined a one-dimensional profile for the quasar, subtracted a stellar PSF, and then fitted the resulting profile with an analytic galaxy model. We have 14 quasars in common. To compare the results, we transform both the

TABLE 9

COMPARISON BETWEEN ABSOLUTE V MAGNITUDES FOR QUASAR HOST GALAXIES EXPECTED FROM K-BAND AND FROM *HST* − F606W MEASUREMENTS

Object	K_{gal}[a]	M_K	$(V-K)$[b]	$M_{V(K)}$	$M_{V(F606)}$(2-D)[c]	ΔM_V
PG 0052+251	15.14	−23.3	3.90	−19.4	−20.9	1.5
PHL 909	14.40	−24.2	3.95	−20.3	−21.0	0.7
PG 0923+201	14.95	−23.9	4.00	−19.9	−21.0	1.1
PG 0953+414	15.28	−24.1	4.20	−19.9	−20.2	0.3
PKS 1004+13	15.12	−24.3	4.20	−20.1	−22.0	1.9
PG 1012+00	13.94	−24.9	4.00	−20.9	−20.7	−0.2
PKS 2135−147.....	14.75	−24.2	4.10	−20.1	−21.1	1.0
PKS 2349−014.....	13.98	−24.7	3.95	−20.8	−22.1	1.3

[a] Dunlop et al. 1993.

[b] $(V-K)$ for elliptical galaxy from Bruzual & Charlot 1993.

[c] This work (derived from two-dimensional galaxy model fitting).

TABLE 10

COMPARISON BETWEEN ABSOLUTE V MAGNITUDES FOR QUASAR HOST GALAXIES EXPECTED FROM H-BAND AND FROM *HST* F606W MEASUREMENTS

Object (1)	H_{gal}[a] (2)	$(V-H)_{normal}$[b] (3)	$M_{V(H)}$ (4)	$M_{V(F606)}$(2-D)[c] (5)	ΔM_V (6)
PG 0052+251	14.46	3.16	−20.8	−20.9	0.1
PG 0923+201	14.86	3.22	−20.8	−21.0	0.2
PG 0953+414	15.38	3.32	−20.7	−20.2	−0.5
PKS 1004+130.....	14.86	3.32	−21.2	−22.0	0.8
PG 1012+008	14.02	3.21	−21.6	−20.7	−0.9
PG 1116+215	13.97	3.20	−21.6	−21.4	−0.2
PG 1202+281	15.07	3.18	−20.3	−20.5	0.2
3C 273	13.01	3.17	−22.3	−22.1	−0.2
PKS 1302−102.....	14.79	3.47	−21.5	−21.1	−0.4
PG 1307+085	15.24	3.16	−20.0	−20.2	0.2
PG 1309+355	14.55	3.21	−21.0	−21.1	0.1
PG 1402+261	14.95	3.18	−20.4	−19.9	−0.5
PG 1444+407	15.19	3.42	−21.0	−20.5	−0.5
3C 323.1	14.80	3.42	−21.4	−21.0	−0.4

[a] McLeod & Rieke 1994b.

[b] McLeod & Rieke 1995.

[c] This work (derived from two-dimensional galaxy model fitting.)

H-band and the F606W magnitudes to the *V* band. We used the *k*-corrections and the relative sensitivities of the different bands calculated by Fukugita et al. (1995) to convert our F606W measurements to *V* (see § 6).

To transform the *H*-band magnitudes to *V*, we assumed $(V-H) \sim 3.0$ for normal galaxies plus a *k*-correction given by McLeod & Rieke (1995). For objects not in their table, we interpolated in redshift to obtain the expected $(V-H)$ for a normal galaxy.

Table 10 lists the following information: column (1): quasar; column (2): McLeod-Rieke *H*-band magnitude for the host galaxy; column (3): color $(V-H)$ for normal galaxies including *k*-correction; column (4): absolute *V* magnitude based on the *H*-band measurements and calculated assuming $H_0 = 100$ km s^{-1} Mpc^{-1}, and Ω_0; column (5): absolute two-dimensional model *V* magnitude estimated from F606W images; and column (6): difference between absolute *V* magnitude estimated from *H*-band and F606W images. The average discrepancy is

$$\langle | M_{V(H)} - M_{V(\mathrm{F606})} | \rangle = 0.4 \pm 0.2 \text{ mag} . \quad (9)$$

For eight of the 14 cases, the McLeod & Rieke luminosities are brighter than the *HST* luminosities. In some cases, the difference is clearly due to the McLeod & Rieke magnitudes also including the companion galaxies (see PG 1012+008 in Figs. 1 and 2 and the discussion in § 9).

9. COMMENTS ON INDIVIDUAL CASES

In this section we will discuss the images of each of the quasars. Table 2 summarizes the morphological information obtained from the *HST* images, and Tables 3–5 give the inferred luminosities of the host galaxies. For comparisons, the absolute magnitudes reported by other authors have been converted to our cosmological parameters. Information about close galaxy companions is summarized in Table 6.

Measurements of the surface brightness along the major axes of the relatively bright elliptical host galaxies of PHL 909, PG 0923+201, PKS 1004+130, HE 1029−140, PG 1116+215, 3C 273, and PKS 2135−147 do not show evidence of discontinuity in the light distribution. Thus, all the apparently elliptical hosts discussed below for which we could make detailed photometry satisfy the criterion of having smooth light distributions. The *HST* images reveal spiral host galaxies with H II regions for three quasars, PG 0052+251, PG 1309+355, and PG 1402+261. It should be feasible to obtain spectra of the brightest H II regions. The spectra may reveal the composition of the material that makes up the quasar hosts and perhaps provide further clues to the quasar phenomenon.

PG 0052+251.—The host is a beautiful spiral galaxy (see Bahcall et al. 1996 for a detailed discussion). The spiral host is evident even in our 200 s exposure. The southern spiral arm extends the farthest from the quasar (in the direction of the companion). There is good agreement between the absolute *V* magnitude estimated from the McLeod & Rieke (1994b) *H*-band image measurements and our two-dimensional model estimate based on the *HST* images. J. Miller (1996, private communication) has recently obtained spectra for some of the bright H II regions identified (Bahcall et al. 1996) in the *HST* images. The H II regions observed have the same redshift as the quasar. The second and third quasar nuclei suggested by Hutchings et al. (1989; the second nucleus was confirmed by Dunlop et al. 1993), are seen on the *HST* images to be, respectively, a bright H II region in the spiral arm of the host galaxy and a foreground star in the Galaxy.

PHL 909 (0054+144).—The quasar host is a normal elliptical E4 galaxy (see Bahcall et al. 1996 for a more extensive discussion and a variety of images). This radio-quiet quasar does not occur in a spiral galaxy, as the conventional view had suggested before the *HST* observations. We did not detect extended emission toward the western companion galaxy, as suggested by Dunlop et al. (1993). The elliptical host is apparent in our 200 s image.

NAB 0205+02.—The appearance of this quasar in the *HST* images (see Fig. 1) resembles, on visual inspection, that of a bright star. Indeed, it is hard to distinguish the quasar from a star by just looking at the images (see Fig. 1). After PSF subtraction, we detect a small disklike host galaxy (see Fig. 2), with size and inclination similar to the companion 8.″3, position angle PA = 332°. The scale length of the host is only ∼1.2 kpc, and the absolute visual magnitude is −19.1.

Figure 3 (Plate 29) compares the host image after subtraction of a blue standard star, MMJ 6481 (see Fig. 3*a*), and after the subtraction of a red standard star, F141 (see Fig. 3*b*). The image of the host galaxy obtained after the subtraction of the PSF for the blue standard star is significantly clearer than the image obtained using the red star PSF. However, there is very little difference quantitatively, <0.1 mag, between the host galaxy magnitudes we determined from the two subtracted images.

Stockton, Ridgway, & Kellogg (1997) recently obtained ground-based images in two line-free continuum bands that show a definite host galaxy elongated roughly northwest-southeast as well as some extended low surface brightness material to the west. In agreement with our results, they report that the host galaxy has about the same luminosity and orientation as the companion in the shorter wavelength image, but the host has somewhat redder colors than the companion. NAB 0205+02 was not resolved in the deep images taken by Smith et al. (1986).

Figure 4 (Plate 30) shows a fascinating object, first noticed by Stockton & MacKenty (1987). The object, which is 12″ to the east of the quasar, is visible in their [O III] image but is absent from their continuum image. It appears as a point source with a bright jetlike structure to the south and a much fainter and curved extension to the north. The width of the jet and of the curved extension is less than 0.3 kpc. The total apparent F606W magnitude of the object is 22.6, and the extension of the jetlike structure and curved tail are 0.″7 (1.2 kpc) and 1.″1 (1.9 kpc), respectively. The offset of this object from the quasar position is $\Delta\alpha = 1.''1$ and $\Delta\delta = 1.''7$.

0316−346.—The morphology of the host environment is complex, probably the result of gravitational interactions with a neighboring galaxy. Figures 1 and 2 show clearly what appear to be tidal tails that extend about 20 kpc west of the quasar. There are also bright diffuse clumps within ∼5 kpc of the quasar, which may contain H II regions. We do not see unambiguous signs of a compact remnant close to the center of light of the quasar. The radial profile is reasonably described by an exponential disk from radius ∼1″ to 6″. There is a relatively bright peculiar spiral galaxy ($m_{606} = 20.7$ mag) projected 26.″7 of the quasar, PA = 67°.

PG 0923+201.—The host of this radio-quiet quasar is an E2 elliptical, a member of a small group of galaxies. The two

galaxies at 11.″0, PA = 151°, and 15.″1, PA = 162°, have redshifts similar to the quasar (Heckman et al. 1984); the companion at 15″ southeast is not shown in Figures 1 and 2. The V magnitude estimated from McLeod & Rieke (1994b) H-band images is in good agreement (0.1 mag) with the magnitude determined from our two-dimensional model.

PG 0953+414.—Low surface brightness fuzz was detected in the early *HST* images (Bahcall et al. 1994, 1995a) and confirmed to be real by longer (Cycle 5) exposures. We are unable to establish the morphology of the fuzz, which is faint and extended. Hutchings et al. (1989) suggested, on the basis of ground-based images, that the host of the quasar has spiral structure and is possibly interacting. The *HST* images do not provide convincing evidence for or against this conjecture. Spectroscopy of the fuzz around the quasar obtained by Boroson et al. (1985) shows that the off-nuclear spectrum is dominated by a red continuum with Hα and possibly [S II] emission; Mg I b absorption might also be present. The absolute V magnitude derived from McLeod & Rieke (1994b) H-band observations is 0.5 mag brighter than our two-dimensional model estimate.

PKS 1004+130.—The host is a bright elliptical, about as bright as the brightest cluster galaxies. There seems to be some structure in the inner region of the host ($r < 2.''5$). The absolute V magnitude derived from McLeod & Rieke (1994b) H-band observations is 0.8 mag fainter than our two-dimensional model estimate. Stockton & MacKenty (1987) presented narrow-band [O III] images of this quasar but did not find any significant extended luminosity in the region between ∼7 to 28 kpc (for $q_0 = 0.5$ and $H_0 = 100$ km s^{-1} Mpc^{-1}). Stockton (1978) obtained spectroscopic observations of the galaxies around the quasar and found that two of them have redshifts similar to the quasar redshift. One of the galaxies is separated by 33.″4 (79.8 kpc, PA = 233°; not shown in Figs. 1 and 2) from the quasar and has $m_{606} = 20.0$ mag; the other is not in our *HST* image field of view.

PG 1012+008.—This quasar is "caught in the act" of merging. The host of this quasar is seen in Figures 1 and 2 to be merging with a bright galaxy. The distance between the two galactic nuclei is 6.7 kpc (3.″3). There is another compact galaxy 6.″8 (12.4 kpc) north of the quasar, probably taking part in the interaction as well. Both interacting companions are also visible in our 200 s exposure.

Figure 5 (Plate 31) shows an expanded view of the PG 1012+008 image. Heckman et al. (1984) obtained spectra for both galaxies and found the expected absorption lines (Hβ, Mg I, Fe II, and Na I) at the same redshift as the quasar. The absolute V magnitude based on the H-band measurement by McLeod & Rieke (1994b) is 0.9 mag brighter than our two-dimensional model estimated value; we believe that part of this discrepancy is caused by the light of the merging galaxy being included in their model fit.

HE 1029−140.—This radio-quiet quasar has a bright elliptical host galaxy. Some faint structures resembling shells are seen at ∼11″ and 19″ from the quasar. There is a compact galaxy 4.″1 north from the quasar; spectroscopy is required to determine if it is associated with the quasar. Wisotzki et al. (1991) obtained R-band images and, based on spheroidal model fits, reported the host to be a giant elliptical with $R = 15.2$ mag and $M_R = -22.0$ mag. Assuming $(V-R) \sim 0.8$ for elliptical galaxies at $z \sim 0.1$ (Fukugita et al. 1995), their absolute V magnitude for the host is −21.2 mag. We obtained $M_V = -20.8$ by fitting a GdV model to the azimuthally averaged profile of the host.

Wisotzki (1994) measured redshifts of galaxies in the field of HE 1029−140 and found that four galaxies have redshifts similar to the quasar. Wisotzki did not detect the close compact object at 4″ projected separation.

The closest galaxy with a redshift known to be similar to the quasar lies at 134 kpc (= 109.″4) PA = 26° and was detected in WF2 (not shown in Figs. 1 and 2). The *HST* images show that this Wisotzki companion galaxy has $M_V \sim -19.1$ ($m_{606} = 17.7$) and is highly disturbed, probably an advanced stage of merger between two disk galaxies. Two possibly galactic nuclei, separated by 1.″4, are visible, as well as H II regions.

There is a $m_{606} = 17.9$ mag galaxy projected at 22.″9, PA = 23°, of the quasar, which Wisotzki showed to be a background galaxy with $z = 0.162$. Wisotzki classified this galaxy as an elliptical, but the *HST* images show that it is a spiral galaxy (type ∼Sab).

PG 1116+215.—The host of this radio-quiet quasar is probably an elliptical galaxy. The bright central region is surrounded by a faint smooth fuzz. Some arclike structures are seen in the center but are almost certainly PSF artifacts. The one-dimensional profile is reasonably described by a de Vaucouleurs model. The V magnitude estimated from McLeod & Rieke (1994b) H-band images is in good agreement with the magnitude determined from our two-dimensional model.

McLeod & Rieke (1995) applied the techniques they developed to study their H-band ground-based images to reanalyze the *HST* Archive images of PG 1116+215. They subtracted just enough of the PSF of the red standard star, F141 ($B-V = 1.11$), from the azimuthally averaged quasar one-dimensional profile to make the residual profile almost turn over in the center. Because the *HST* images were saturated in the center, McLeod & Rieke normalized the light profile just outside the saturation region. We note, however, that the region inside $r \sim 2''$ is heavily contaminated by PSF artifacts when the PSF of the red star F141 is used for the subtraction. If F141 is used for the PSF subtraction, there are artificial radial spikes—which are not visible in their published *HST* image of this quasar. McLeod & Rieke state that the host of PG 1116+215 "looks nearly identical" to a field galaxy detected in WF4. An *HST* image of this field galaxy was published in Bahcall et al. (1995a, Fig. 5*c*). The field galaxy is rich in morphological details: it is a barred spiral with internal and external rings (RSBb). If it is at the same distance as the quasar, its absolute V magnitude is −20.9. Although the host and the field galaxy have apparently similar luminosities, they are morphologically quite different.

PG 1202+281.—The host of this radio-quiet quasar, also known as GQ Com, is a small elliptical E1 galaxy. Stockton & MacKenty (1987) showed that the compact galaxy ∼5″ from the quasar, PA = 71°, is at the same redshift as the quasar. Boroson et al. (1985) reported that the off-nuclear spectra are dominated by a red continuum, with [O III] lines and possibly Hα in emission, and a possible Mg I b absorption feature. The V magnitude estimated from the McLeod & Rieke (1994b) H-band images is in good agreement with the magnitude determined by our two-dimensional model.

3C 273 (PG 1226+023).—The host galaxy is an elliptical. The V magnitude estimated from the McLeod & Rieke

(1994b) H-band images is in good agreement with the magnitude determined by our two-dimensional model. Using deep ground-based CCD images, Tyson et al. (1982) obtained $M_V \sim -22.5$ for the host, which is in good agreement with our best two-dimensional model magnitude of $M_V = -22.1$. The host is somewhat brighter than the brightest galaxy in a rich cluster. Stockton (1980) measured redshifts for galaxies in the 3C 273 field and found that four of them have redshifts similar to the quasar, in agreement with the suggestion of Bahcall & Bahcall (1970). One of those galaxies was detected (a spiral galaxy) in WF4: it lies at 75″ east of the quasar (∼133 kpc), and its redshift is $z = 0.1577$. Wyckoff et al. (1981) obtained $R = 16.3$ for the host, which is equivalent to $M_V \sim -21.3$ mag. The inner part of the jet is barely visible in the PSF-subtracted image in Figure 2. *HST* and Merlin observations of the 3C 273 jet are reported in Bahcall et al. (1995d).

PKS 1302−102.—The *HST* images show there are two small compact galaxies at 1″ and 2″ from the quasar, which are expected to spiral into the quasar in a time short compared to the Hubble time (Bahcall et al. 1995a). The presence of these very close companions can be seen most clearly in the expanded image, Figure 8, of Bahcall et al. (1995a). Hutchings & Neff (1992) performed optical imaging with 0.″5 resolution and reported structures at the positions of those galaxies; they suggest the host is a mildly disturbed elliptical galaxy. The PSF-subtracted residual image (see Fig. 2) appears to the eye to be similar to an elliptical galaxy, but an exponential disk fits the data slightly better. The absolute V magnitude estimated for the host galaxy is 0.4 mag fainter than the value determined from the McLeod & Rieke (1994b) H-band observations and is 0.9 mag fainter than the value estimated from i-band images (Véron-Cetty & Woltjer 1990). Wyckoff et al. (1981) obtained $R = 19.0$ for the host; using the Fukugita et al. (1995) transformations of galaxy colors, this corresponds to $M_V \sim -20.0$.

PG 1307+085.—The host appears to be a small early-type galaxy. The absolute V magnitude estimated from our two-dimensional model of the *HST* image is 0.2 mag fainter than the value derived from the McLeod & Rieke H-band images.

PG 1309+355.—Figure 6 (Plate 32) shows an expanded view of the image for PG 1309+355 with lower contrast than shown in Figures 1 and 2. The details near the center of PG 1309+355 are shown more clearly in Figure 6, after a best-fit stellar PSF has been subtracted. This quasar has a bright early-type host galaxy, probably an Sab. Tightly wrapped spiral arms are clearly seen in the inner region surrounding the center of the quasar. Overall, the GdV model describes the radial profile better than the exponential disk model. The absolute V magnitude estimated from our two-dimensional model of the *HST* image is 0.1 mag brighter than the value derived from the McLeod & Rieke (1994b) H-band images.

PG 1402+261.—Figure 7 (Plate 33) shows an expanded view of the image of this quasar at two different contrast levels. The *HST* images show that the host is a beautiful spiral. After the PSF subtraction, a bar and a possible inner ring are visible. The morphological type is approximately SBb(r?). H II regions are also visible along one of the spiral arms; they are less prominent than the H II regions seen in the spiral host of PG 0052+251. The relative positions and magnitudes of the brightest H II regions are marked for identification in the upper panel in Figure 7. Table 11 lists for each H II region the aperture magnitude, the distance to the quasar nucleus, and the offset in right ascension and declination between the H II region and the quasar nucleus. The magnitudes were measured using apertures of 0.″3.

TABLE 11

H II REGIONS IN THE HOST GALAXY OF PG 1402+261

Region	m_{F606W}	d (arcsec)	$\Delta\alpha$ (arcsec)	$\Delta\delta$ (arcsec)
a	23.7	2.8	−0.3	2.8
b	24.3	2.9	−1.5	2.5
c.....	25.3	2.9	−2.1	2.0
d	25.6	3.5	−3.3	1.3
e.....	25.5	4.6	−4.5	−0.9
f.....	26.2	4.8	−4.5	−1.8
g	26.2	5.0	−4.2	−2.8
h	25.9	5.3	−3.8	−3.7
i.....	25.6	4.1	−1.1	4.0
j.....	25.2	4.0	−2.7	3.0

PG 1402+261 is a relatively isolated quasar. Stockton & MacKenty (1987) did not find any significant extended [O III] emission around the quasar. McLeod & Rieke (1994b) obtained H-band images; the absolute V magnitude based on their measurement is 0.5 mag brighter than the value estimated with our two-dimensional model of the *HST* images.

PG 1444+407.—The host galaxy of this quasar is smooth and is elongated in the north-south direction. After the PSF subtraction, the nuclear region is seen as an extended structure running northeast-soutwest, as shown in Figure 2. A bar may be present. The exponential disk model describes the radial light distribution a little better than does the GdV model. The overall appearance is most similar to an E2 galaxy. Hutchings & Neff (1992) originally suggested the possibility of a bar in this host, which they proposed might be in an advanced stage of the merger of galaxies of very different masses. The absolute V magnitude estimated from our two-dimensional model of the *HST* image is 0.5 mag fainter than the value derived from the McLeod & Rieke H-band images.

3C 323.1 (PG 1545+210).—A low surface brightness elliptical host galaxy appears in the *HST* images, as well a neighboring companion at a projected distance of ∼7 kpc, (2.″7, PA = 292°) (see Figs. 1 and 2). The V magnitude of the host galaxy determined from the H-band images by McLeod & Rieke (1994b) is 0.4 mag brighter than the value derived from our two-dimensional model of the *HST* images. More recently, Neugebauer, Matthews, & Armus (1995) obtained H- and K-band images of 3C 323.1; their estimated model fit H-band magnitude for the host agrees with the results of McLeod & Rieke (1994b). The measurements of Neugebauer et al. suggest that if the host galaxy is a normal elliptical, its expected apparent V magnitude is ∼17.5, and if it is a spiral galaxy, $V \sim 16.9$. These values are brighter than the V-band apparent magnitudes expected using a color transformation without reddening of our *HST* images (see Table 4) but are consistent with the host galaxy being a reddened elliptical, as pointed out by Neugebauer et al. (1995). The GdV one-dimensional model fits better the surface brightness radial profile of the quasar host in our *HST* image than does the exponential disk model.

Stockton (1982) took spectra of the companion galaxy at 2.″7 from the quasar and apparently detected [O III] at the same redshift as the quasar. Complex, asymmetric extended

[O III] emission is seen surrounding the quasar in [O III] images obtained later by Stockton & MacKenty (1987). However, there is no excess of emission at the companion galaxy position in the [O III] images. Stockton & MacKenty conclude that the previously reported detection of [O III] emission in the spectrum of the companion galaxy was fortuitous, since the emission is due to the general distribution of ionized gas surrounding the quasar. Neugebauer et al. found that the H and K model fit magnitudes obtained for the companion galaxy, when combined with the *HST* measurements by Bahcall et al. (1995a), give a color $V-H$ consistent with the companion galaxy being a faint elliptical at the redshift of the quasar.

PKS 2135−147.—The quasar host is an elliptical galaxy; the envelope is not featureless like PHL 909 but rather contains some faint clumps. The image suggests the presence of a jet at PA $\sim 26°$, with visual extension of $\sim 2\farcs4$ and width $\sim 0\farcs5$. The surface brightness of the jetlike feature is 23.4 mag arcsec^{-2} (F606W), at $1\farcs7$ from the quasar center of light. Many galaxies are seen in the field; the closest companions to the quasar are at $1\farcs9$, PA = 128°, and $5\farcs5$, PA = 119°, seen in Figures 1 and 2. Stockton (1978, 1982) obtained spectra of the field galaxies and found that four are at the same distance as the quasar, including the closest companions at projected separations of $1\farcs9$ and $5\farcs5$. Somewhat later, Stockton & MacKenty (1987) obtained [O III] images. They noted that the companion 2″ southeast did not appear enhanced in the [O III] images, indicating that the emission lines seen in the combined spectrum are due to extended emission around the quasar that is not confined to the companion. Hickson & Hutchings (1987) reported Mg b in the spectrum of the secondary nucleus (the galaxy at 2″ southeast) corresponding to a galaxy at the redshift of the quasar.

PKS 2135−147 has been included in many imaging programs. For example, Dunlop et al. (1993) measured $M_K(\text{host}) = -24.2$, which gives $M_V \sim -21.0$. Our two-dimensional model analysis of *HST* images gives $M_V \sim -21.1$. Véron-Cetty & Woltjer (1990) obtained i-band images and measured aperture photometry in an annulus with radii 12.5 and 25 kpc. They estimated $M_V = -19.9$. We measured the absolute magnitude of the host in our *HST* images within the same annulus and obtained $M_V \sim -19.4$. Smith et al. (1986) measured the absolute blue magnitude to be $M_B \sim -21.5$, which converts to $M_V \sim -19.9$ [if $(B-V) \sim 1.6$ for an elliptical galaxy at $z = 0.2$]. Wyckoff et al. (1981) obtained $R = 17.8$, which corresponds to $M_V \sim -19.3$.

PKS 2349−014.—The quasar host galaxy is undergoing gravitational interaction, which is evidenced by apparently tidal arms and possibly also by a huge (~ 50 kpc) diffuse off-center nebulosity. A compact companion galaxy at 2″ east is detected in the *HST* images. Bahcall et al. (1995b, 1995c) provide an extensive discussion of this object and include a number of different images (the tidal wisps and extended nebulosity are seen most clearly in their Figs. 1 and 2; the close companion galaxy is featured in their Fig. 3). Dunlop et al. (1993) suggest that the quasar is interacting with the three closest galaxies southeast of the quasar. The *HST* images do not show evidence for this interaction; the three galaxies do not seem to be morphologically disturbed, and no obvious link between them and the quasar is seen. Dunlop et al. measured $M_K(\text{host}) = -24.7$, which gives $M_V \sim -21.5$. Our two-dimensional model fits to the *HST* image of the host give $M_V \sim -22.0$, similar to the light from a brightest cluster galaxy.

The radial profile of the interacting system PKS 2349−014 is well described by a de Vaucouleurs model. As pointed out by Toomre (1995) and Bahcall et al. (1995b), there are some morphological resemblances between PKS 2349−014 and NGC 3921. Schweizer (1996) has carefully and extensively studied NGC 3921, suggesting that it is the result of a merger between two disk galaxies and is now a protoelliptical. In this case also, the mean light distribution of the system is well described by a $r^{1/4}$ law.

10. SUMMARY AND DISCUSSION

The images shown in Figures 1 and 2 establish the two main conclusions of this paper: (1) The most luminous nearby quasars exist in a variety of environments; (2) *HST* observations provide unique information about the circumstances of the quasar phenomenon. Many of the most important results obtained in this paper are visible on the unprocessed images shown in Figure 1, which can be compared with the images with a stellar PSF subtracted shown in Figure 2. The subtraction of a stellar PSF is important in about half of the cases.

Our results are based upon a representative sample of 20 of the most luminous known ($M_V < -22.9$) and nearby ($z < 0.30$) quasars. The characteristics of the sample are summarized in Table 1 and § 2.1.

In separate subsections, we summarize and discuss below our results on host morphologies, host luminosities, comparisons with our earliest analyses, close companions, ground-based studies, and future work.

10.1. *Host Morphologies*

Figures 1 and 2 show three hosts that apparently are normal spirals with H II regions (PG 0052+251, PG 1309+355, and PG 1402+261), seven ellipticals (PHL 909, PG 0923+201, PKS 1004+130, HE 1029−140, PG 1116+215, 3C 273, and PKS 2135−147), as well as three obvious cases of current gravitational interaction (0316−346, PG 1012+008, and PKS 2349−014). There are also five other hosts that appear to be elliptical galaxies and are listed as En(?) in Table 2. The hosts for two of the quasars (NAB 0205+02 and PG 0953+414) are faint and difficult to classify.

The host galaxies are centered on the quasars to the accuracy of our measurements, ± 0.4 kpc (see § 6 and eq. [6]).

Seven of the 14 radio-quiet quasars in our sample occur in hosts that are classified as elliptical galaxies in Table 2. Two particularly beautiful examples of elliptical hosts for radio-quiet quasars are shown in Figures 1 and 2 for PHL 909 and HE 1029−140. We have presented a more extensive discussion of the host of PHL 909 in Bahcall et al. (1996). Five of the six radio-loud quasars in our sample appear to lie in elliptical galaxies. The sixth radio-loud quasar, PKS 2349−014, is in a complex interacting system containing a close companion, apparent tidal tails, and a large off-center nebulosity.

The fact that about half of the radio-quiet quasars in our sample have elliptical hosts contradicts the conventional wisdom that radio-quiet quasars occur in spiral galaxies. However, we confirm the expectation that most radio-loud quasars are in elliptical galaxies.

Three of the quasars in our sample, 0316−346, PG 1012+008, and PKS 2349−014, have been "caught in the

act," i.e., the *HST* images of these quasars show dramatic evidence of currently intense gravitational interactions. Two of the three quasars caught in the act are radio quiet. In all three cases, the unprocessed images (see Fig. 1) are sufficient to reveal extended curved features that look like the tidal arms generated in numerical simulations of interacting galaxies. For 0316−346 and PKS 2349−014, there is no clear evidence for a normal host galaxy centered on the quasar. PG 1012+008 appears to be an example of a merger currently going on between two comparable galaxies. For a more extensive analysis of PKS 2349−014, the reader is referred to Bahcall et al. (1995b, 1995c), in which the close companion, the tidal arms, the very extended off-center nebulosity, and the possible host galaxy are all discussed in some detail.

The *HST* images provide the best database to search for optical jets in nearby, luminous quasars. Information on the existence or nonexistence of small-scale optical jets can constrain theories of the origin of radio and optical jets. We examined the images of all 20 of the quasars for the existence of optical jets. With the exception of the well-known jet in 3C 273, the only other quasar for which we have found evidence for linear features is PKS 2135−147. Sensitive radio searches should be undertaken to test whether PKS 2135−147 has a radio jet. For the other quasars, we can rule out the existence of a narrow optical feature with a surface brightness in excess of 24.5 mag s^{-2} extending more than 3 kpc beyond an inner region beginning at about 6 kpc.

10.2. *Host Luminosities*

We list in Table 12 our best estimates for the magnitudes of the host galaxies in our sample; these magnitudes were obtained (see § 5.3) by fitting a two-dimensional analytic galaxy model to the data. We also list the effective radius or exponential scale length and give the morphology of the host based on visual inspection of the images (see Table 2 and § 3). The different measurements of the brightnesses of the host environments are summarized and compared in Tables 3 and 4 and in § 6. The average best-fit two-dimensional model magnitudes for the hosts of the 14 radio-quiet quasars is

$$\langle M_V \rangle_{\text{model, radio-quiet}} = -20.6 \pm 0.6 \text{ mag} . \quad (10)$$

The hosts of the six radio-loud quasars are slightly brighter,

$$\langle M_V \rangle_{\text{model, radio-loud}} = -21.6 \pm 0.6 \text{ mag} . \quad (11)$$

The fact that in our sample the radio-loud quasars are, on the average, about a magnitude brighter than the radio-quiet quasars cannot be explained by a selection effect resulting from the fact that the radio-loud quasars have a slightly larger average redshift. In fact, the three radio-loud quasars with $z \leq 0.20$ have $\langle M_V \rangle = -21.8$ mag, and the three radio-loud quasars with $0.20 < z < 0.30$ have $\langle M_V \rangle = -21.4$ mag.

Figure 8 shows the two-dimensional model absolute visual magnitudes (from Table 12) of the host galaxies (and other nebular material) versus the absolute visual magnitudes of the quasars. In order to be detectable, the host must have a luminosity that is not too small when compared with the luminosity of the quasar. The minimum detectable host brightness depends strongly upon the assumed morphology of the host galaxy. We have shown by a series of numerical experiments, described in Table 3 of Paper II, that host galaxies are, on the average, visible on our images down to about 4.2 mag fainter than the quasar luminosity.

Galaxies that are smooth ellipticals are the most difficult to detect (see rows 5d and 5e of Table 3 of Paper II). For the eight quasars discussed in Paper II, smooth elliptical hosts are, on average, visible on our images down to 3.5 ± 0.5 mag fainter than the quasar. The limiting brightnesses were determined by visually inspecting simulated galaxies placed in the actual *HST* quasar observations and are therefore somewhat subjective.

The diagonal line in Figure 8 represents the detection limit for smooth ellipticals in an idealized sample in which

TABLE 12

SUMMARY OF MAGNITUDES AND MORPHOLOGY FOR QUASAR HOST GALAXIES

		TWO-DIMENSIONAL			
OBJECT	z	m_{606}(2-D)	M_V(2-D)	r (arcsec)[a]	MORPHOLOGY
PG 0052+251	0.155	17.2	−20.9	1.3	Sb
PHL 909	0.171	17.2	−21.0	2.3	E4
NAB 0205+02	0.155	19.0	−19.1	0.7	S0?
0316−346	0.265	18.3	−20.8	1.2	Inter.
PG 0923+201	0.190	17.5	−21.0	2.9	E1
PG 0953+414	0.239	18.8	−20.2	1.1	?
PKS 1004+130.....	0.240	16.9	−22.0	1.2	E2
PG 1012+008	0.185	17.7	−20.7	1.6	Inter.
HE 1029−140	0.086	16.2	−20.5	3.2	E1
PG 1116+215	0.177	16.9	−21.4	1.4	E2
PG 1202+281	0.165	17.7	−20.5	1.4	E1
3C 273	0.158	16.0	−22.1	3.7	E4
PKS 1302−102.....	0.286	18.2	−21.1	1.1	E4?
PG 1307+085	0.155	17.8	−20.2	1.3	E1?
PG 1309+355	0.184	17.3	−21.1	1.2	Sab
PG 1402+261	0.164	18.3	−19.9	1.6	SBb
PG 1444+407	0.267	18.4	−20.5	1.0	E1?
3C 323.1	0.266	18.1	−21.0	1.6	E3?
PKS 2135−147.....	0.200	17.4	−21.1	2.6	E1
PKS 2349−014.....	0.173	16.2	−22.1	4.8	Inter.

[a] Effective radius or exponential scale length.

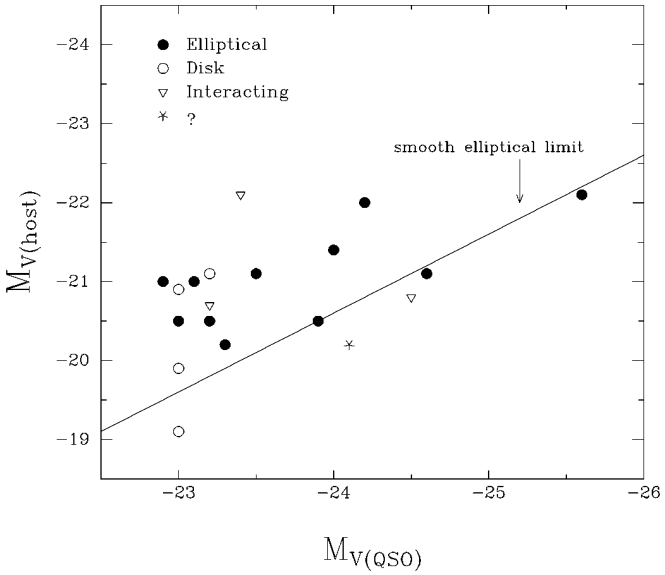

FIG. 8.—Absolute visual magnitude of the host galaxies vs. the absolute visual magnitude of the quasars. The magnitudes and morphologies of the host galaxies are determined using two-dimensional fits (see the summary in Table 12); the absolute magnitudes of the quasars are taken from Table 1. The diagonal line represents the average detection limit of smooth ellipticals in an idealized sample; see the discussion in § 10.2.

the limiting host magnitude is determined entirely by the quasar luminosity. In calculating the limiting absolute visual magnitudes for the hosts, we have included an average k-correction (see Fukugita et al. 1995) for ellipticals at $z = 0.2$, as well as the average magnitude difference, 3.1 mag, between the quasar and the faintest detectable host. Thus

$$M_{\text{limiting host}} = M_{\text{QSO}} + \Delta \, . \tag{12}$$

The form of equation (12) reflects the fact that the limiting host luminosity must increase linearly with the luminosity of the quasar, since by assumption the noise introduced by the quasar signal determines how faint a host can be detected. Smooth ellipticals fainter than ± 0.5 mag of the diagonal line in Figure 8 would not have been expected to be detected if this idealization of the problem is correct. For the three intrinsically faintest quasars in our sample, the noise introduced by the quasar, the host galaxy, and the background light are all similar. In practice, for our sample one might expect some flattening of the detection limit at the lowest quasar luminosities if photon noise is more important than systematic uncertainties in the subtraction of the quasar light.

McLeod & Rieke (1995) have suggested that there is a linear relation between the quasar absolute magnitude and the minimum host galaxy absolute magnitude. They interpret this linear relation, shown in their Figure 2, as indicating that a more luminous host galaxy is required to fuel a more luminous quasar. The linear relation that they find between M(host) and M(QSO) is essentially identical to our minimum detection limit for smooth ellipticals that is shown in Figure 8 (for $V-H = 3.0$). As pointed out by McLeod (1996), the relation described by McLeod & Rieke cannot be an artifact produced by detection limits if all of their detections are real detections; an artificial correlation would be introduced only if true nondetections were interpreted as marginal detections.

There is not convincing evidence in Figure 8 for a significant dependence of host luminosity upon the luminosity of the quasar. The apparent correlation that is suggested to the eye is due in large part to the fact that the single most luminous quasar in our sample, 3C 273, has the most luminous host.

There is a hint in Figure 8 that the average luminosity of elliptical hosts is somewhat higher than for spiral hosts. Most of this difference, however, is due to the fact that, even for the same objects (see Table 4), the de Vaucouleurs fitting formula yields estimated luminosities that are 0.6 mag brighter than the disk fitting function. The de Vaucouleurs formula introduces a luminosity peak in the unmeasured region that is not present in the disk formula.

Our results are inconsistent with the hosts having a Schechter luminosity function. The average absolute magnitude for a field galaxy is about 1.8 mag fainter than $M_V(L^*) = -20.5$ [for an assumed minimum luminosity of $M_V(L^*) = -17$; see, e.g., Efstathiou, Ellis, & Peterson 1988 for a discussion of the field galaxy luminosity function]. In our sample (see Table 12 and Fig. 8), the average host is $M_V(L^*) = -20.9$. Moreover, about half by number of the field galaxies would be expected, in a volume-limited sample, to lie within a magnitude of the lower limit cutoff of the Schechter luminosity function [which may be fainter than $M_V(L^*) = -17$]. Thus, if the host galaxies were distributed with a Schechter luminosity function, we would have expected that about half of the hosts in our sample would be fainter than $M_V(L^*) = -18$ and therefore undetectable on the *HST* images. This is clearly not the case.

By comparing the two-dimensional model magnitudes of Table 12 and Figure 8 with the results expected from a Schechter luminosity function, we conclude that, on average, the host galaxies of the luminous quasars in our sample are about 2.2 mag more luminous than typical field galaxies.

10.3. *Previous Analyses*

The conclusions presented in this summary paper are different in emphasis from the conclusions in our first two studies (see Papers I and II). In our earlier work, we discussed images of eight quasars (all are included in the sample in the current work) and reported the definitive detection of three host galaxies. We also presented limits on the brightnesses of the hosts for the other five quasars. The images presented in this paper show that more than half of the entire sample of 20 quasars has obvious hosts and that there is solid evidence that most, if not all, of the remaining quasars also have host galaxies.

The initial caution that we expressed regarding the detection of host galaxies was due to a combination of the unlucky observing sequence and our conservatism about interpreting the complex *HST* images. The unprocessed *HST* data (see Fig. 1) are sufficient to show, even to the untrained eye, that at least nine of the 20 quasars in our sample have obvious hosts or diffuse environments. These obvious examples include the three spiral hosts (PG 0052+251, 1309+355, and PG 1402+261), the three quasars "caught in the act" (0316−346, PG 1012+008, and PKS 2349−014), and three prominent ellipticals (PHL 909, HE 1029−140, and 3C 273). None of these quasars were among the first four objects (PG 0953+414, PG 1116+215, PG 1202+281, and PG 1307+085) observed (Paper I), and only one (3C 273, whose host we described in

Paper II together with the original observations) belonged to the sample of eight quasars (Paper II). With a probability of 9/20 per observation of observing an obvious host, it was simply bad luck (about a 5% chance) that only one of the initial eight quasars studied in Paper I and Paper II had an obvious host.

Given the repaired, but still complex and temporally variable, PSF of the *HST*, we presented our results (see Table 3 of Paper II) for the nondetections as a morphology-dependent limit on the brightness of the host galaxy. Spiral galaxies, with their azimuthal variation in brightness and regions of high surface brightness, could be seen to considerably fainter total brightnesses (more than a magnitude) than large, extended ellipticals with their smooth, regular profiles. As we have gained experience with the data, we have become more confident of our ability to judge the reality of low surface brightness features. Most importantly, during *HST* Observation Cycle 5, we obtained additional images of PG 0953+414, a quasar analyzed in Paper I that showed very faint, extended nebulosity that was not centered on the quasar. The Cycle 5 observations were obtained at a different roll angle than those described in Paper I; the new observations confirmed the reality of the diffuse features (the nebulosity remained fixed in the sky when the telescope was rotated). The observations of PG 0953+414 suggested that some of the faint features that we had initially worried could be PSF features were real.

In retrospect, it appears that the vast majority of our initial observations consisted of quasars whose hosts had smooth, regular profiles. Comparing our adopted brightnesses of the hosts (Table 12) with the brightness limits set in our earlier work by simulations (Table 3 in Paper II), we find that the appropriate brightnesses limits (those for smooth ellipticals like 5d and 5e of Fig. 5 of Paper II) were reasonably accurate. The detected brightnesses reported in Table 12 of this paper range from considerably fainter than the Paper II limit (e.g., PG 0953+414) to slightly brighter than the limit (e.g., 3C 323.1). Since the morphology of the hosts of the initial quasars was biased toward one type of galaxy (the least favorable type as far as detectability), it was not accurate, as we did, to quote a detection limit that was the average of all the galaxy types.

10.4. *Close Companions*

The *HST* images frequently reveal companion galaxies that are projected very close to the quasar, in some cases as close as 1″ or 2″. Table 6 shows 20 galaxy companions that are projected closer than 25 kpc to the center of light of a quasar and brighter than $M(\mathrm{F606W}) = -16.4$. Altogether, 13 of the 20 quasars in our sample have close companions that satisfy the requirements for inclusion in Table 6. The amplitude for the quasar-galaxy correlation function determined from our data is 3.8 ± 0.8 times larger than the galaxy-galaxy correlation function (Fisher et al. 1996).

10.5. *Ground-based Studies*

Our results for individual objects are compared in § 8 with the results from previous ground-based observations. In general, the agreement with ground-based observations is satisfactory but not as precise as we would have hoped. The most straightforward comparison is with the results of Véron-Cetty & Woltjer (1990) in annular regions well separated from the quasar. Even in this case, our *HST* magnitudes are, on average, 0.4 mag fainter than the Véron-Cetty & Woltjer values. Our two-dimensional model estimates for the total luminosities are, on average, 0.8 mag fainter than their one-dimensional model fits. The average discrepancy between our results and those of Dunlop et al. (1993) is 1.0 ± 0.6 mag (our results are generally brighter than those of Dunlop et al.), and the average discrepancy between our results and those of McLeod & Rieke is 0.4 ± 0.2 mag.

10.6. *Future Work*

Some pre-*HST* theoretical analyses (e.g., by Falle, Perry, & Dyson 1981, Weymann et al. 1982, Begelman 1985, and Chang, Schiano, & Wolfe 1987) have suggested that luminous quasars may have dramatic effects on their environments via the radiation or hot winds that the quasar emits. The continuum images shown in this paper do not provide obvious evidence for the effects of the quasar on the host environment. In fact, the three spiral host galaxies and several of the host ellipticals appear remarkably normal. Broadband colors and spectroscopic observations are required in order to determine more sensitively whether the host galaxy is really oblivious to the presence of the luminous quasar in its center. The theoretical modeling can now be made more specific and compared with the results of the *HST* observations for individual host galaxies. These studies will be important in constraining the timescale of the quasar phenomenon and the isotropy of the quasar emissions. If a quasar shines brightly for only a short period of time or if the emission is highly anisotropic, then the lack of a dramatic effect of the bright AGN on the surrounding medium may be more easily understood.

One of the key results that is apparent in Figures 1 and 2 is the detailed evidence for gravitational interactions among the systems "caught in the act" (0316−346, PG 1012+008, and PKS 2349−014). Dynamical modeling of these systems could provide insights into the processes involved in the formation and fueling of quasars.

HST images provide detailed quantitative information about the environments in which the quasar phenomenon occurs. We hope to increase our sample in the future and to obtain color information about the objects discussed here. It should be feasible to obtain spectra of the brightest H II regions in the spiral hosts of PG 0052+251, PG 1309+355, and PG 1402+261. Detailed comparisons between the *HST* and ground-based images will be very informative.

We are grateful to P. Crane, M. Fall, O. Gnedin, K. Kellermann, K. McLeod, J. Miller, G. Neugebauer, M. Rees, G. Rieke, and M. Strauss for valuable discussions, comments, and suggestions. J. Krist and C. Burrows constructed the four stellar PSFs used in this work; we are grateful to them for their skill and generosity in providing these data. We would like to thank Digital Equipment Corporation for providing the DEC4000 AXP Model 610 system used for the computationally intensive parts of this project. This work was supported in part by NASA contract NAG 5-1618, NAG 5-3259, NASA grant NAGW-4452 and grant GO-5343 from the Space Telescope Science Institute, which is operated by the Association of Universities for Research in Astronomy, Incorporated, under NASA contract NAS 5-26555. We have used the NASA/IPAC Extragalactic Database (NED), operated by the Jet Propulsion Laboratory, Caltech, under contract with NASA, and NASA's Astrophysics Data System Abstract Service (ADS).

REFERENCES

Bahcall, N., & Bahcall, J. N. 1970, PASP, 82, 1276
Bahcall, J. N., et al. 1993, ApJS, 87, 1
Bahcall, J. N., Kirhakos, S., & Schneider, D. P. 1994, ApJ, 435, L11 (Paper I)
———. 1995a, ApJ, 450, 486 (Paper II)
———. 1995b, ApJ, 447, L1 (Paper III)
———. 1995c, ApJ, 454, L175 (Erratum)
———. 1996, ApJ, 457, 557
Bahcall, J. N., Kirhakos, S., Schneider, D. P., Davis, R. J., Muxlow, T. W. B., Garrington, S. T., Conway, R. G., & Unwin, S.C. 1995, ApJ, 452, L91 (Paper IV)
Begelman, M. C. 1985, ApJ, 297. 492
Boroson, T. A., Persson, S. E., & Oke, J. B. 1985, ApJ, 293, 120
Bruzual A., G., & Charlot, S. 1993, ApJ, 405, 538
Burrows, C. J. 1994, *Hubble Space Telescope* Wide Field and Planetary Camera 2 Instrument Handbook, Version 2.0 (Baltimore: Space Telescope Science Institute)
Chang, C. A., Schiano, A. V. R., & Wolfe, A. M. 1987, ApJ, 322, 180
de Vaucouleurs, G. 1948, Ann. d'Ap., 11, 247
Disney, M. J., et al. 1995, Nature, 376, 150
Dunlop, J. S., Taylor, G. L., Hughes, D. H., & Robson, E. I. 1993, MNRAS, 264, 455
Efstathiou, G., Ellis, R. S., & Peterson, B. A. 1988, MNRAS, 232, 431
Falle, S. A. E. G., Perry, J. J., & Dyson, J. E. 1981, MNRAS, 195, 397
Fisher, K. B., Bahcall, J. N., Kirhakos, S., & Schneider, D. P. 1996, ApJ, 468, 469
Fukugita, M., Shimasaku, K., & Ichikawa, T. 1995, PASP, 107, 945
Gehren, T., Fried, J., Wehinger, P. A., & Wyckoff, S. 1984, ApJ, 278, 11
Heckman, T. M., Bothun, G. D., Balick, B., & Smith, E. P. 1984, AJ, 89, 958
Hickson, P., & Hutchings, J. B. 1987, ApJ, 312, 518
Hoessel, J. G., & Schneider, D. P. 1985, AJ, 90, 1648
Holtzman, J. A., et al. 1995a, PASP, 107, 156
———. 1995b, PASP, 107, 1065
Hutchings, J. B. 1987, ApJ, 320, 122
Hutchings, J. B., Crampton, D., Campbell, B., Gower, A. C., & Morris, S. C. 1982, ApJ, 262, 48
Hutchings, J. B., Holtzman, J., Sparks, W. B., Morris, S. C., Hanisch, R. J., & Mo, J. 1994, ApJ, 429, L1
Hutchings, J. B., Janson, T., & Neff, S. G. 1989, ApJ, 342, 660
Hutchings, J. B., & Morris, S. 1995, AJ, 109, 1541
Hutchings, J. B., & Neff, S. G. 1992, AJ, 104, 1
Jannuzi, B. T., et al. 1997, in preparation
Kellermann, K. I., Sramek, R. A., Schmidt, M., Green, R. F., & Shaffer, D. B. 1994, AJ, 108, 1163
Kirshner, R. F., Oemler, A., Schechter, P. L., & Shectman, S. A. 1983, AJ, 88, 1285
Krist, J., & Burrows, C. 1994, WFPC2 Instrument Science Report 94-01 (Baltimore: Space Telescope Science Institute)
Krist, J., & Burrows, C. 1996, http://www.sns.ias.edu/jnb (go to HST Images)
Kristian, J. 1973, ApJ, 179, L61
Malkan, M. A. 1984, ApJ, 287, 555
Malkan, M. A., Margon, B., & Chanan, G. A. 1984, ApJ, 280, 66
McLeod, K. K. 1996, private communication
McLeod, K. K., & Rieke, G. H. 1994a, ApJ, 420, 58
———. 1994b, ApJ, 431, 137
———. 1995, ApJ, 454, L77
Montgomery, K. A., Marschall, L. A., & Janes, K. A. 1993, AJ, 106, 181
Neugebauer, G., Matthews, K., & Armus, L. 1995, ApJ, 455, L123
Postman, M., & Lauer, T. R. 1995, ApJ, 440,28
Romanishin, W., & Hintzen, P. 1989, ApJ, 341, 41
Sandage, A. 1961, The Hubble Atlas of Galaxies (Washington: The Carnegie Institution of Washington)
Schechter, P. 1976, ApJ, 203, 297
Schweizer, F. 1996, AJ, 111, 109
Smith, E. P., Heckman, T. M., Bothun, G. D., Romanishin, W., & Balick, B. 1986, ApJ, 306, 64
Stockton, A. 1978, ApJ, 223, 747
———. 1980, in IAU Symp. 92, Objects of High Redshift, ed. G. O. Abell & P. J. E. Peebles (Dordrecht: Reidel), 89
———. 1982, ApJ, 257, 33
Stockton, A., & MacKenty, J. W. 1987, ApJ, 316, 584
Stockton, A., Ridgway, S., & Kellogg, M. 1997, in preparation
Toomre, A. 1995, private communication
Trauger, J. T., et al. 1994, ApJ, 435, L3
Tyson, J. A., Baum, W. A., & Kreidl, T. 1982 ApJ, 257, L1
Véron-Cetty, M. P., & Véron, P. 1991, A Catalogue of Quasars and Active Nuclei (ESO Sci. Rept. No. 10) (5th ed.; Garching: ESO)
———. 1996, A Catalogue of Quasars and Active Nuclei (ESO Sci. Rept.) (7th ed.; Garching: ESO), in press
Véron-Cetty, M. P., & Woltjer, J. 1990, A&A, 236, 69
Weymann, R. J., Scott, J. S., Schiano, A. V. R., & Christiansen, W. A. 1992, ApJ, 262, 497
Wisotzki, L. 1994, A&A, 292, 45
Wisotzki, L., Hagen, H., Hopp, U., & Reimer, D. 1991, in Physics of Active Galactic Nuclei, ed. W. J. Duschl & S. J. Wagner (Berlin: Springer), 438
Wyckoff, S., Gehren, T., Morton, D. C., Albrecht, R., Wehinger, P. A., & Boksenberg, A. 1980, ApJ, 242, 59
Wyckoff, S., Wehinger, P. A., & Gehren, T. 1981 ApJ, 247, 750
Yee, H. K. C. 1987, AJ, 94, 1461